PAPER

Oxidative desulfurization of model oil in an organic biphasic system catalysed by Fe₃O₄@SiO₂–ionic liquid

Abdolhamid Alizadeh, [ID] *[ab] Mitra Fakhari,[a] Mohammad Mehdi Khodaei,[a] Gisya Abdi[a] and Jhaleh Amirian[c]

Lewis or Brønsted acidic methylimidazolium ionic liquid-functionalized Fe₃O₄@SiO₂ nanoparticles were fabricated and applied as an efficient magnetic heterogeneous catalyst for dibenzothiophene (DBT) oxidation in a biphasic system using H_2O_2 as the oxidant. The structures of catalysts were characterized by SEM, TEM, XRD, TGA, FT-IR, VSM and EDX techniques. The magnetic catalysts showed high catalytic performance in the oxidation of DBT in an *n*-hexane/acetonitrile biphasic system using H_2O_2, and high conversions were obtained. The effects of contact time, temperature, amount of H_2O_2 and amount of catalyst on the DBT oxidative removal efficiency were investigated. The contact time of 60 min, 0.1 g catalyst, and 4 mL H_2O_2 at 313 K were found as optimal experimental conditions for an improved DBT oxidative removal process. The sulfur level could be lowered from 100 ppm to less than 7, 5, and 2 ppm under optimal conditions for Fe₃O₄@SiO₂–Mim-BF₄, Fe₃O₄@SiO₂–Mim-HSO₄, and Fe₃O₄@SiO₂–Mim–FeCl₄, respectively. These nanomagnetic heterogeneous catalysts could be easily separated from the reaction mixture by applying an external magnetic field and recycled several times.

1. Introduction

Emission of SO_x from the combustion of sulfur compounds in gasoline and diesel oil is one of the issues of concern in the environmental field. Hence, sulfur removal from fuel oils is a crucial challenge from an environmental point. To eliminate sulfur-containing compounds, various processes, have been employed. Generally, the processes include catalytic hydro-desulfurization,[1] adsorption,[2,3] extraction,[4,5] bioprocesses,[6,7] and oxidation processes.[8–12]

In industry, the removal of sulfur compounds is carried out by the hydrodesulfurization (HDS) method, which requires harsh condition such as high temperatures and high pressures of hydrogen gas to produce light oil having low levels of sulfur compounds. Thus according to this point oxidative desulfur-ization (ODS) is taken into consideration owing to favorable operating conditions.

Generally, ODS processes are achieved through oxidation of sulfur compounds to sulfoxides and sulfones followed by a separation process using appropriate extractants or adsorbents.[13–15] According to the literature, various oxidative desulfurization systems have been developed[16] such as a series of heteropolyacid catalysts,[17] ionic liquids systems, acetic acid catalyst,[18,19] the amphiphilic phosphotungstic acid catalyst,[20] porous glass supported with titanium silicate particles,[21] and ultrasound-assisted oxidative desulfurization processes.[22]

Recently, due to their superior properties including good dissolving ability, nonvolatility, and wide liquid temperature range, ionic liquids (ILs) have become an active area of research. They have been employed as solvents for synthesis and catal-ysis,[23] in electrochemistry,[24] extractive[25] and oxidative desulfur-ization.[26] In the field of desulfurization in some cases, ionic liquids act as both catalyst and extractant, simultaneously. Some of these ILs are reported as catalysts and extractant for extractive-catalytic-oxidative-desulfurization (ECODS), including *N*-methyl-2-pyrrolidone-based ionic liquids,[27] dialkylpyridinium tetra-chloroferrates [C$_n$³MPy] FeCl₄ (n = 4, 6, 8),[28] [C₄Mim]Cl/MCl₂ (M = Zn, Fe, Cu, Mg, Sn, Co),[29] [Hnmp]BF₄,[30] [BMim]HSO₄,[31] [BMim][HSO₄], and [C₄Py][HSO₄].[32] These biphasic systems exhibit some disadvantages, such as high cost, large usage amount of IL, difficult separation and recontamination of oils from the dissolution of traces of catalysts. To overcome these limitations, supported ILs on the various materials as hetero-geneous catalysts have been introduced because they not only decrease the cost and the usage amount of ILs but also facilitate separation and recycling of the catalyst. Various kinds of nano-materials as supports to fix of ionic liquids have been applied such as SiO_2, Al_2O_3 and TiO_2 nanoparticles,[33] a series of polymer-

[a] Department of Organic Chemistry, Faculty of Chemistry, Razi University, Kermanshah, 6714967346 Iran. E-mail: ahalizadeh2@hotmail.com; ahalizadeh2@razi.ac.ir; Fax: +98 833 427 4559; Tel: +98 833 427 4559

[b] Nanoscience & Nanotechnology Research Center (NNRC), Razi University, Kermanshah, Iran

[c] Department of Regenerative Medicine, College of Medicine, Soonchunhyang University, 366-1, Sangyong-dong, Cheonan-City, Republic of Korea

based materials,[5] mesoporous materials,[34,35] metal–organic frameworks,[36] and graphene-based materials.[37] Also, magnetic Fe_3O_4 nanoparticles have been used as support for ionic liquids. Ionic liquid modified magnetic nanoparticles have been used as catalyst for chemical synthesis,[38–40] oxidative desulfurization[11,41,42] and adsorbent.[43,44]

Besides, magnetic catalysts in recent years have been faced with a lot of attention. Meanwhile, magnetic ionic liquids[45,46] are applied as extractants and catalysts for desulfurization of model oils.

In this research, for the achievement of magnetically separable catalyst with high catalytic performance, we planned to fabricate and use modified magnetic nanoparticles by Lewis or Brønsted acidic ionic liquids as catalysts for oxidation of dibenzothiophene (DBT) by H_2O_2 in a biphasic (n-hexane/acetonitrile) system.

2. Experimental

2.1 Materials

Ferric chloride hexahydrate ($FeCl_3 \cdot 6H_2O$), ferrous chloride tetrahydrate ($FeCl_2 \cdot 4H_2O$), sodium tetrafluoroborate ($NaBF_4$), sodium hydrogen sulfate ($NaHSO_4$), iron(III) chloride ($FeCl_3$), tetraethylorthosilicate (TEOS), (3-chloropropyl)trimethoxysilane (CPTS), 1-methyl imidazole were purchased from Sigma-Aldrich. Ammonia, acetonitrile, n-hexane, toluene, and ethanol were procured from Merck. All other reagents used in this study were analytical grade and distilled or double distilled water was used in the preparation of all solutions.

2.2 Analysis instruments

X-ray diffraction (XRD) spectra were recorded on D/MAX-250, Rigaku, Tokyo, Japan using 40 kV with Cu Kα irradiation (λ = 1.541 Å). Fourier transform infrared (Bruker FTIR) spectra were recorded in KBr pellets in the range of 400–4000 cm^{-1}. Scanning electron microscopy (SEM) images of the product were taken using a JSM-6701F microscope (JEOL, Japan) equipped for EDS. Transmission electron microscopy (TEM) was performed on JEOL JEM-1010n. The magnetic measurements were carried out in a vibrating sample magnetometer (VSM, BHV-55, Riken, Japan) at room temperature. Thermogravimetric analysis (TGA) was carried out using a Q5000IR (TA instruments) under nitrogen flow (100 mL min^{-1}) with ramp rate of 10 °C min^{-1}. UV-visible spectra were recorded by Perkin Elmer Lambda 25 spectrometer.

2.3 Methods

2.3.1 Synthesis and modification of magnetic nanoparticles. Iron oxide magnetic nanoparticles were prepared according to a reported procedure.[47] Regularly 15 mL of ammonium hydroxide 28% under rapid mechanical stirring was quickly added to the solution of iron(III) chloride hexahydrate (10 mmol) and iron(II) chloride tetrahydrate (5 mmol) that dissolved in distilled water (100 mL) in Ar atmosphere and then the mixture was heated up to 60 °C for 1 h under argon atmosphere. Finally, synthesized nanoparticles were collected by a magnet, and was washed with water and acetone and was dried at room temperature.

2.3.2 Synthesis of silica-coated magnetic nanoparticles ($Fe_3O_4@SiO_2$). Following the Stöber method with some modifications,[48] 1 g of prepared Fe_3O_4 nanoparticles were redispersed in 50 mL of distilled water by the ultrasonic treatment for 20 min. The resultant suspension and 5 mL of $NH_3 \cdot H_2O$ were poured into 150 mL of ethanol with vigorous stirring at 40 °C. Finally, under continuous mechanical stirring, 1 mL of TEOS (tetraethylorthosilicate) diluted in 20 mL ethanol was
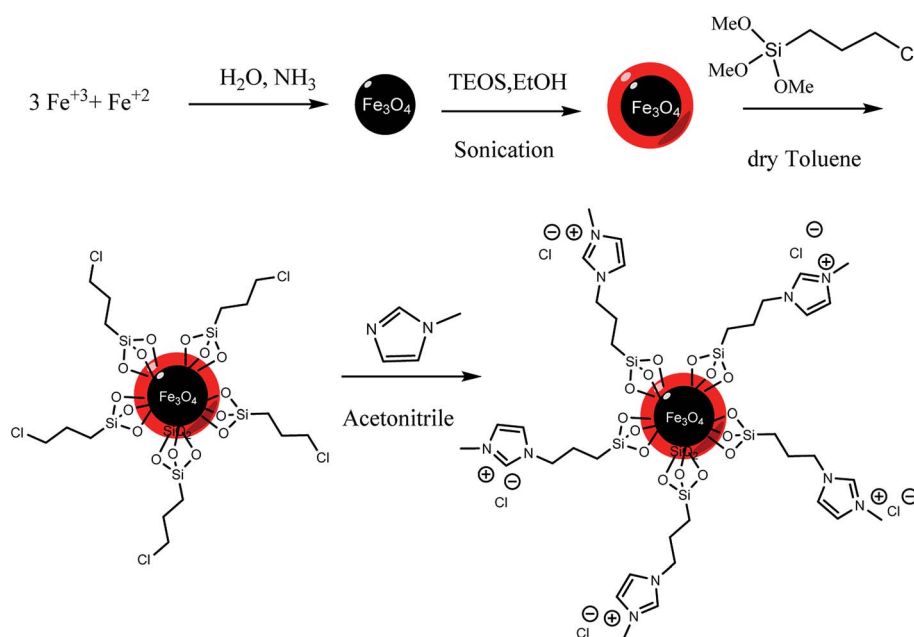
Scheme 1 Preparation of $Fe_3O_4@SiO_2$–methylimidazolium chloride.

dropwise added to this dispersion. The resulting dispersion was kept stirred mechanically for 24 h at room temperature. The magnetic $Fe_3O_4@SiO_2$ nanoparticles were collected by a magnet and washed with ethanol and deionized water in sequence.

2.3.3 Synthesis of ionic liquid-modified silica-coated magnetic nanoparticles. First, chloropropyl-modified silica-coated magnetic nanoparticles were prepared following the modified procedure of Zeng *et al.*[49] 1 mL (5 mmol) of CPTS ((3-chloropropyl)tri-methoxysilane) was dissolved in 100 mL of dry toluene, then 1 g of $Fe_3O_4@SiO_2$, was added to this mixture and this solution was heated to 60 °C and stirred for 18 h. Synthesized $Fe_3O_4@SiO_2$–Cl was washed with toluene and collected by a magnet, and was dried in vacuum. The prepared $Fe_3O_4@SiO_2$–Cl (1 g) and 0.4 mL (5 mmol) of 1-methyl imidazole were mixed in acetonitrile (50 mL) in a round-bottom flask, and the mixture was stirred under reflux condition for 24 h. The obtained product was collected magnetically from the solution and washed copiously with water and ethanol and was dried at 80 °C (Scheme 1).

3. Results and discussion

3.1 Characterization of catalyst

The morphology of $Fe_3O_4@SiO_2$–methylimidazolium chloride nanoparticles was studied by transmission electron microscopy (SEM) shown in Fig. 1a. The TEM observation indicates that magnetite nanoparticles are monodispersed and have an average diameter ranging about 10–15 nm (Fig. 1b).

The crystalline structure of $Fe_3O_4@SiO_2$–methylimidazolium chloride nanoparticles was identified with XRD technique (Fig. 2). For silica and ionic liquid coated Fe_3O_4, diffraction peaks with 2θ at 30.4°, 35.6°, 43.3°, 53.7°, 57.3°, and 62.8°, indicative of a cubic spinel structure of the magnetite were observed which conforms well to the reported value, implying the formation of a Fe_3O_4 phase.[50] The presence of a broad peak at 20–28° is in good agreement with the amorphous structure of silica layer.[47]

TGA analyses of the nanoparticles were also used to determine the percent of organic functional groups chemisorbed onto the surface of $Fe_3O_4@SiO_2$–methylimidazolium chloride. Fig. 3 represents the TGA of as-prepared $Fe_3O_4@SiO_2$–methylimidazolium chloride. The weight loss at temperatures below 100 °C can be attributed to the water desorption from the surface of silica layer.[51] Complete loss of all the covalently attached organic structure is seen in the 200–600 °C temperature range leaving SiO_2, and the organic fraction corresponds to 8.5% weight of the ionic liquid modified silica.[52] These results prove that the attachment of imidazolium moiety onto the surface of the $Fe_3O_4@SiO_2$ nanoparticle.

The FTIR spectra (Fig. 4) certified the structure of $Fe_3O_4@SiO_2$–$Fe_3O_4@SiO_2$–methylimidazolium chloride. The observed signal at 579 cm^{-1} is ascribed to the Fe–O bond vibration. In the case of $Fe_3O_4@SiO_2$–Cl nanoparticles (curve *b*), the sharp band at 1090 cm^{-1} is corresponding to Si–O–Si antisymmetric stretching vibration, being indicative of the existence of a SiO_2 layer around the Fe_3O_4 nanoparticles.[53] The peaks in *b* and *c* at 1633 cm^{-1} and 2930 cm^{-1} were due to the –C=N–, and C–H
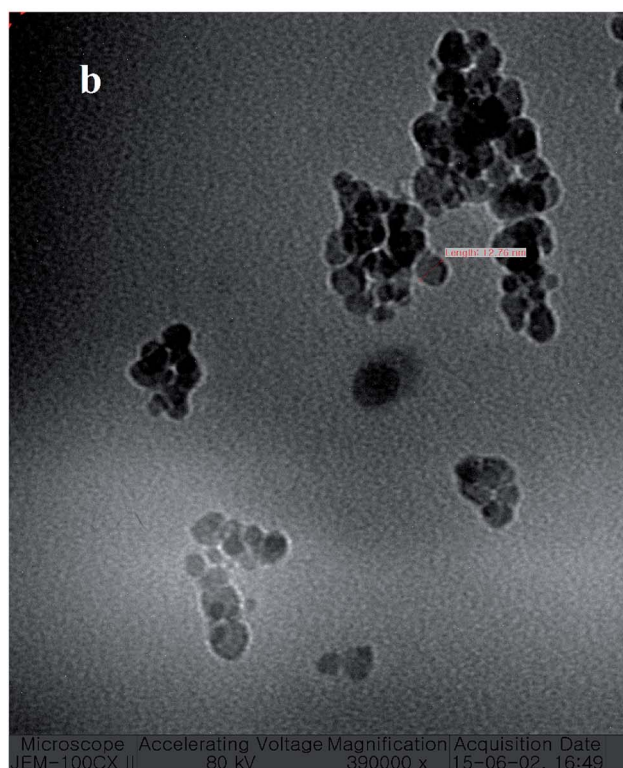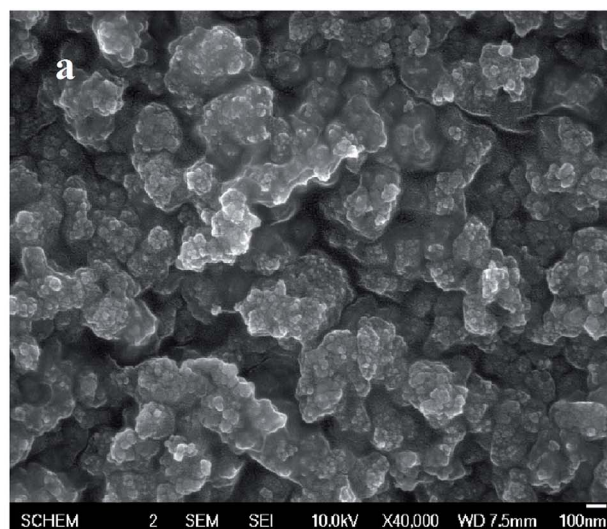

Fig. 1 (a) SEM image of $Fe_3O_4@SiO_2$–methylimidazolium chloride and (b) TEM image $Fe_3O_4@SiO_2$–methylimidazolium chloride.

groups, respectively.[43] Furthermore, the broad absorption in the region of 3445 cm^{-1} is due to the Si–OH groups on the surface of the silica. These results demonstrated the successful bonding of imidazolium ring to the magnetic nanoparticles by covalent bonds.

The magnetic property of ionic liquid supported magnetic nanoparticles was characterized by a vibrating sample magnetometer (VSM) and Fig. 5 shows the typical room temperature magnetization curve of Fe_3O_4 and $Fe_3O_4@SiO_2$–methylimidazolium chloride nanoparticles. The saturation magnetization (M_s) of the $Fe_3O_4@SiO_2$–methylimidazolium chloride is
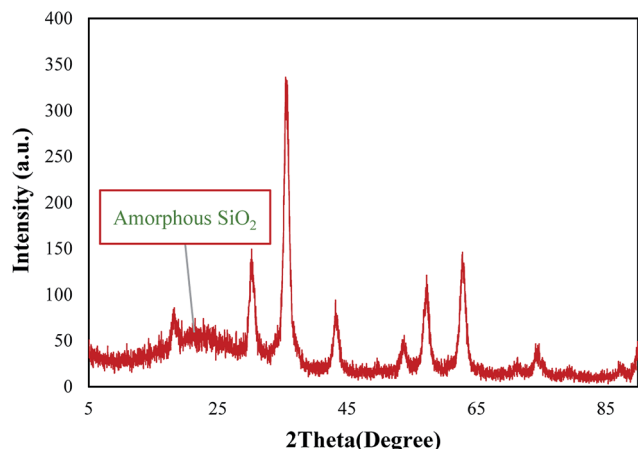
Fig. 2 XRD patterns of the catalyst (Fe₃O₄@SiO₂−methylimidazolium chloride).

Fig. 4 FT-IR spectrum of (a) Fe₃O₄ (b) Fe₃O₄@SiO₂−Cl (c) Fe₃O₄@-SiO₂−methylimidazolium chloride.

Fig. 3 TGA curves of the catalyst (Fe₃O₄@SiO₂−methylimidazolium chloride).
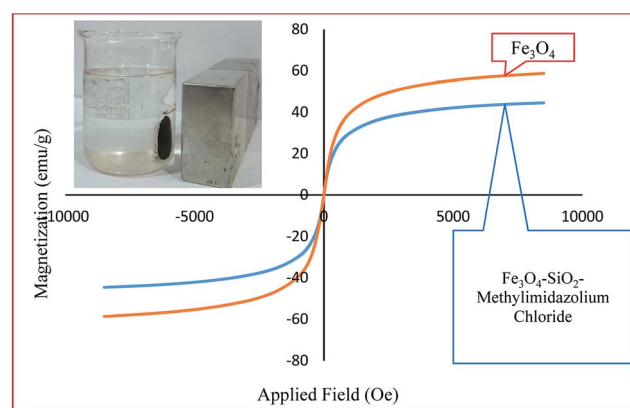
Fig. 5 Hysteresis loops of the Fe₃O₄ and Fe₃O₄@SiO₂−methylimidazolium chloride nanoparticles.

43 emu g^{-1} (Fig. 5), indicating the high magnetic property. As seen in Fig. 5 the M_s of Fe₃O₄ is 59 emu g^{-1}. The lower saturation magnetization of the Fe₃O₄@SiO₂−methylimidazolium chloride compared to the Fe₃O₄ could be ascribed to the attached organic layer to the surface of Fe₃O₄ nanoparticles. The left inset of Fig. 5 shows that Fe₃O₄@SiO₂−methylimidazolium chloride is attracted by an external magnet, and the clear biphasic system can be easily removed by pipet or decanting.

3.2   Anion exchange process

3.2.1   Preparation of Fe₃O₄@SiO₂−methylimidazolium tetrafluoroborate (Fe₃O₄@SiO₂−Mim-BF₄). The anion of the chloride containing ionic liquids was exchanged according to literature (Scheme 2).[54] The (0.5 g) ionic liquid supported magnetic nanoparticles was dispersed in (30 mL) water and (1 g, 10 mmol) sodium tetrafluoroborate were added to the mixture. The reaction mixture was stirred for 30 minutes and then (30 mL) dichloromethane was added. The anion exchanged ionic liquid supported magnetic nanoparticles were transferred to the organic phase. The anion exchanged ionic liquid supported
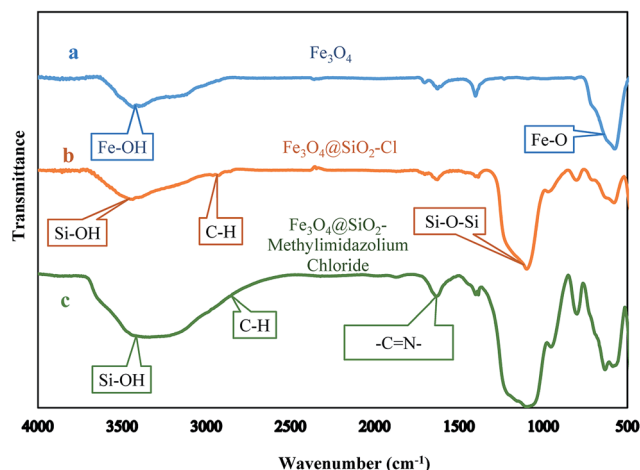
magnetic nanoparticles were collected by external magnetic field and was decanted. The product was washed with deionized water several times for removal of additional NaBF₄ and dry at room temperature. As shown in Fig. 6a, energy-dispersive X-ray spectroscopy of catalyst confirms the presence of the desirable elements in the structure of the catalyst, *i.e.* B, F, N, C.

3.2.2   Preparation of Fe₃O₄@SiO₂−methylimidazolium hydrogen sulfate (Fe₃O₄@SiO₂−Mim-HSO₄). The synthetic process of Fe₃O₄@SiO₂−methylimidazolium hydrogen sulfate is shown in Scheme 2. Fe₃O₄@SiO₂−methylimidazolium chloride (0.5 g) and NaHSO₄ (1.4 g, 10 mmol) were added into a 100 mL water in 150 mL round-bottom flask, and the mixture was stirred at room temperature for 24 h. The magnetic solid was collected by an external magnet and was washed with water several times for removal of additional NaHSO₄ and dried at room temperature. Energy-dispersive X-ray spectroscopy from the attained catalyst confirms the presence of the probable element in the structure of the catalyst, *i.e.* S, C, N (Fig. 6b).

3.2.3   Preparation of Fe₃O₄@SiO₂−methylimidazolium chloride–FeCl₃ (Fe₃O₄@SiO₂−Mim–FeCl₄). The synthetic
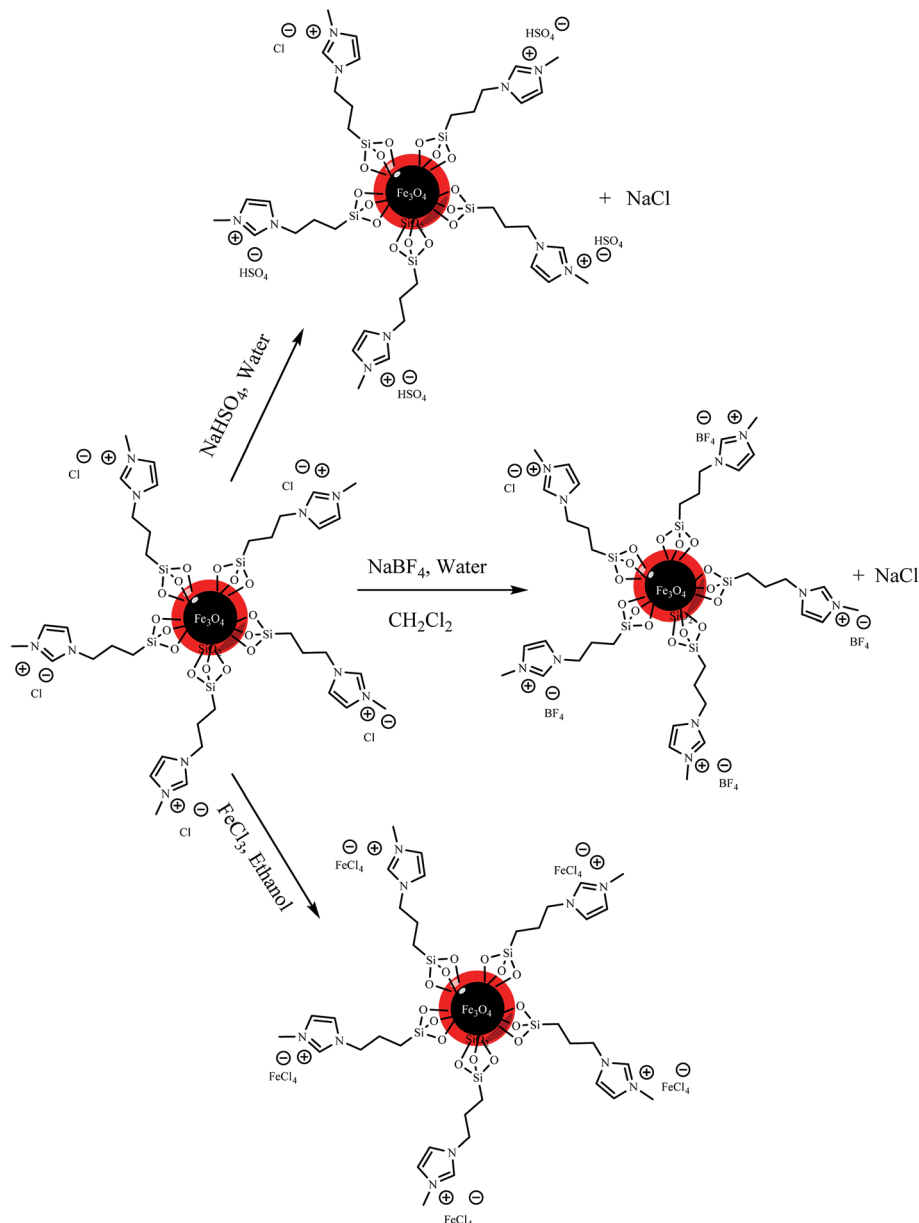
Scheme 2 Schematic illustration of $Fe_3O_4@SiO_2$–methylimidazolium chloride nanoparticles anion exchange.

process of $Fe_3O_4@SiO_2$–methylimidazolium chloride–$FeCl_3$ is shown in Scheme 2. Following the Wang *et al.* method with some modifications[5] $Fe_3O_4@SiO_2$–methylimidazolium chloride (0.5 g) and $FeCl_3$ (1.6 g, 10 mmol) were added into 100 mL ethanol as solvent, and this mixture was stirred for 24 h at room temperature. The solid was collected by external magnetic field and was washed with ethanol and dried at room temperature. As shown in Fig. 6c energy-dispersive X-ray spectroscopy (EDX) of catalyst confirm the presence of the favorable elements in the structure of the catalyst, *i.e.* Fe, Cl, C, N. As seen in the Table 1, increase of wt% of iron and chlorine in $Fe_3O_4@SiO_2$–Mim–$FeCl_4$ compared with $Fe_3O_4@SiO_2$–Mim-BF_4 and $Fe_3O_4@SiO_2$–Mim-HSO_4 confirm the presence of $FeCl_4^-$ moiety on the surface of magnetic nanoparticles (Scheme 3).

3.3 Oxidation procedure

Model oils were prepared by dissolving DBT in *n*-hexane give solutions with a sulfur content of 100 ppm. The extraction and catalytic oxidative desulfurization experiments were performed in a stirred 100 mL round-bottom flask, to which catalyst and model oil (25 mL) and acetonitrile (25 mL) as extractant phase were added in turn. Until the extractive equilibrium was reached after 10 min, a certain amount of 30 wt% H_2O_2 was injected to the flask. Then the mixture was stirred vigorously at 40 °C for 60 min. The concentrations of DBT were analyzed using a UV spectrophotometer. The phase fractional was taken from *n*-hexane phase for DBT analysis. In during the reaction time in intervals 10 min the model oil was separated by decantation after collection of the catalyst by external magnetic
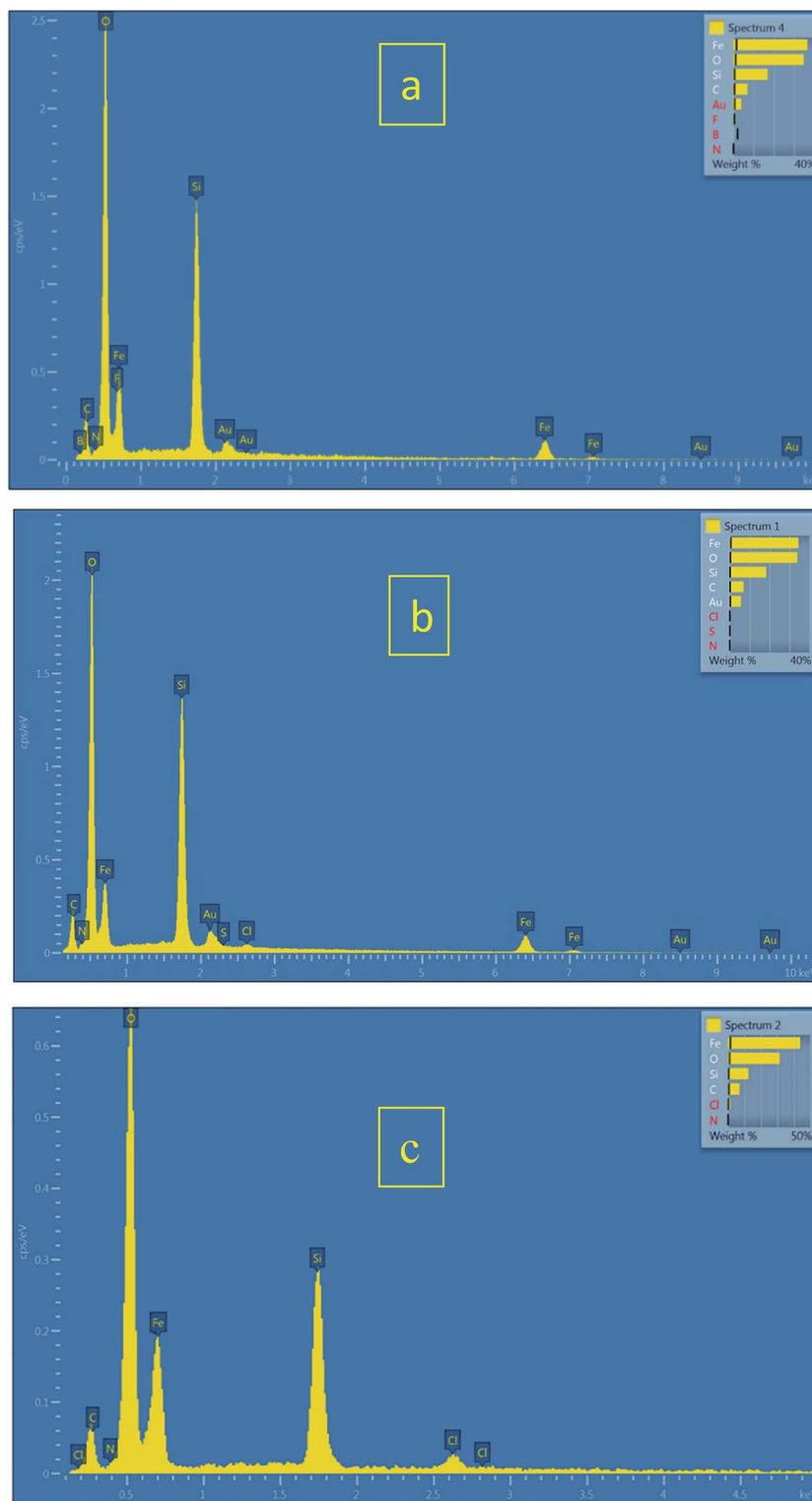
Fig. 6 Energy dispersive X-ray spectroscopy of (a) $Fe_3O_4@SiO_2-Mim-BF_4$ (b) $Fe_3O_4@SiO_2-Mim-HSO_4$ and (c) $Fe_3O_4@SiO_2-Mim-FeCl_4$.

field then the sulfur concentration in oil phase calculated *via* UV-VIS spectrophotometer. The absorption at 283 nm was used to monitor the DBT concentration. Fig. 7 shows the variations of the UV-vis spectra of the DBT in *n*-hexane at time intervals 10, 20, 30, 40, 50, 60 min. The decrease of intensity in these UV-vis

bands, indicates that the concentration of DBT in *n*-hexane decreases during the reaction time. Dibenzothiophene sulfone formation in acetonitrile phase was monitored by thin-layer chromatography (TLC). Sulfone formation was confirmed by the melting point of the obtained product (229–232 °C).
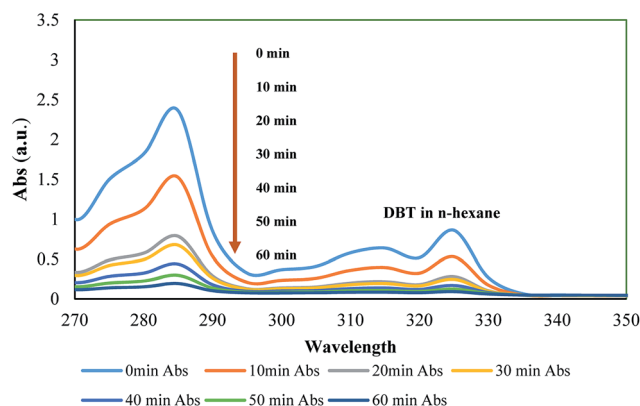
Table 1 Quantitative EDS analyses of the element proportion in catalysts

Element	Weight%		
	Fe$_3$O$_4$@SiO$_2$–Mim-BF$_4$	Fe$_3$O$_4$@SiO$_2$–Mim-HSO$_4$	Fe$_3$O$_4$@SiO$_2$–Mim–FeCl$_4$
Fe	34.87	32.50	43.95
O	34.90	33.97	31.47
Si	17.01	18.30	12.44
C	7.01	6.98	7.08
N	1.83	2.01	2.02
Cl	—	0.40	3.04
F	0.38	—	—
B	0.08	—	—
S	—	0.19	—
Au	3.92	5.64	—
Total	100	100	100

Fig. 7 The variations of the UV-vis spectra of the DBT at time intervals: 10, 20, 30, 40, 50, 60 minutes.

3.4 Control experiments

To evaluate the performance of ionic liquid-modified silica-coated magnetic nanoparticles as catalysts in the oxidation of DBT from a biphasic system, we set four parallel control experiments to make a comparison on the performance of Fe$_3$O$_4$@SiO$_2$, Fe$_3$O$_4$@SiO$_2$–Cl, Fe$_3$O$_4$@SiO$_2$–imidazolium chloride and Fe$_3$O$_4$@SiO$_2$–Mim–FeCl$_4$ as catalysts. The obtained data was shown in Table 2. As can be seen in Table 2 conversion of dibenzothiophene to dibenzothiophene sulfone was not observed. These observations were contributed to this fact that on the surfaces of Fe$_3$O$_4$@SiO$_2$, Fe$_3$O$_4$@SiO$_2$–Cl and Fe$_3$O$_4$@-SiO$_2$–methylimidazolium chloride nanoparticles does not exist necessary sites for activation of H$_2$O$_2$.

The presence of the ionic liquid moieties on the surface of magnetic nanoparticles leading to high polarity of the catalyst surface and the polar catalyst could be easily dispersed in acetonitrile phase. First DBT influenced from nonpolar n-hexane phase to the polar acetonitrile phase. On the other hand, H$_2$O$_2$ as an oxidant could be easily adsorbed to the polar surface of the catalyst and then the oxidation process continues.
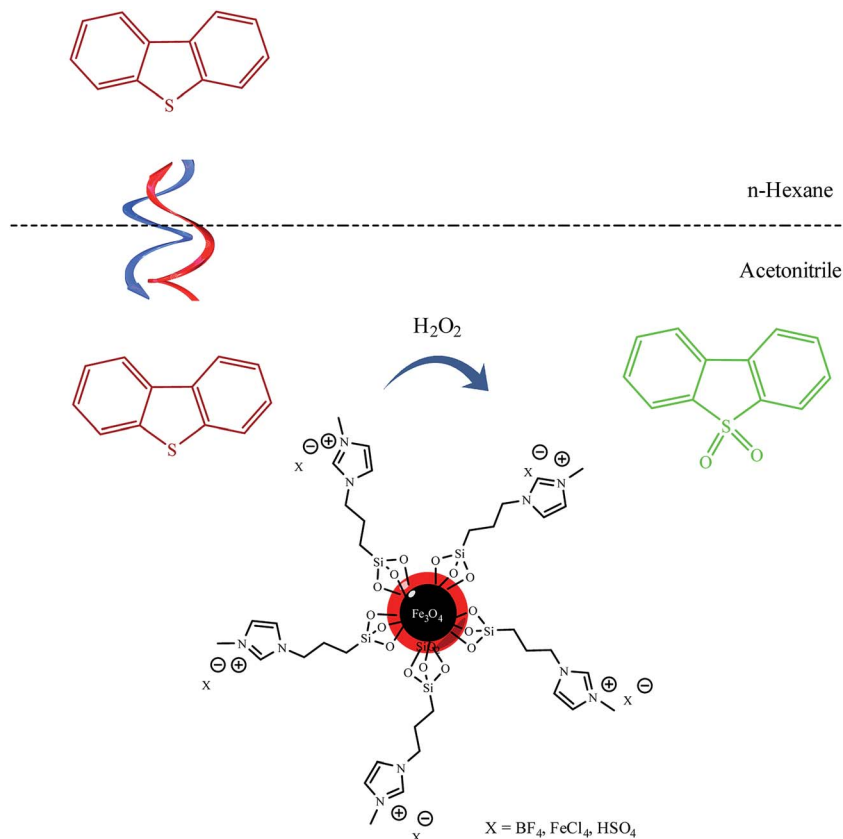

Scheme 3 The oxidation of DBT to sulfone catalyzed by Fe$_3$O$_4$@SiO$_2$–methylimidazolium chloride.

Table 2 Comparison of the performance of $Fe_3O_4@SiO_2$, $Fe_3O_4@$-SiO_2–Cl, $Fe_3O_4@SiO_2$–methylimidazolium chloride and $Fe_3O_4@SiO_2$–Mim–FeCl$_4$ as catalyst[a]

Catalyst	Dispersity in acetonitrile	Conversion%
$Fe_3O_4@SiO_2$	✓	0
$Fe_3O_4@SiO_2$–Cl	✓	0
$Fe_3O_4@SiO_2$–methylimidazolium chloride	✓✓✓	0
$Fe_3O_4@SiO_2$–Mim–FeCl$_4$	✓✓✓	98

[a] Experimental conditions: amount of catalyst: 0.1 g, amount of H_2O_2: 4 mL, time: 60 minutes, temperature: 313 K.

3.5 The proposed process and mechanism of DBT oxidation by $Fe_3O_4@SiO_2$–Mim-BF$_4$

The proposed mechanism of DBT oxidation by $Fe_3O_4@SiO_2$–Mim-BF$_4$ nanocatalyst was shown in Scheme 4. As can be seen, the efficiency of the oxidation can be explained by the interaction between the $Fe_3O_4@SiO_2$–Mim-BF$_4$ and H_2O_2. The boron of anionic moiety of the catalyst can attract H_2O_2 and increases the electrophilic ability of a peroxy oxygen atom of H_2O_2 and the electrophilic oxygen is attacked by sulfur of DBT. After eliminating

one water molecule, dibenzothiophene sulfoxide is produced. In continuous by cooperation of catalyst and oxidant, oxidation process continues and dibenzothiophene sulfone is produced.

3.6 The suggested process and mechanism of DBT oxidation by $Fe_3O_4@SiO_2$–Mim-HSO$_4$

According to the last researches[31,55,56] about oxidation of sulfides by Brønsted acidic catalysts, the proposed mechanism for the oxidation of sulfide to the corresponding sulfoxide is shown in Scheme 5. The efficiency of the oxidation can be explained by the interaction between the $Fe_3O_4@SiO_2$–Mim-HSO$_4$ and H_2O_2. The OH moiety of the $Fe_3O_4@SiO_2$–Mim-HSO$_4$ forms a strong hydrogen bond with H_2O_2 and increases the electrophilic ability of a peroxy oxygen atom of H_2O_2, and at the same time assists the leaving group (H_2O) in departing from the reaction intermediate.
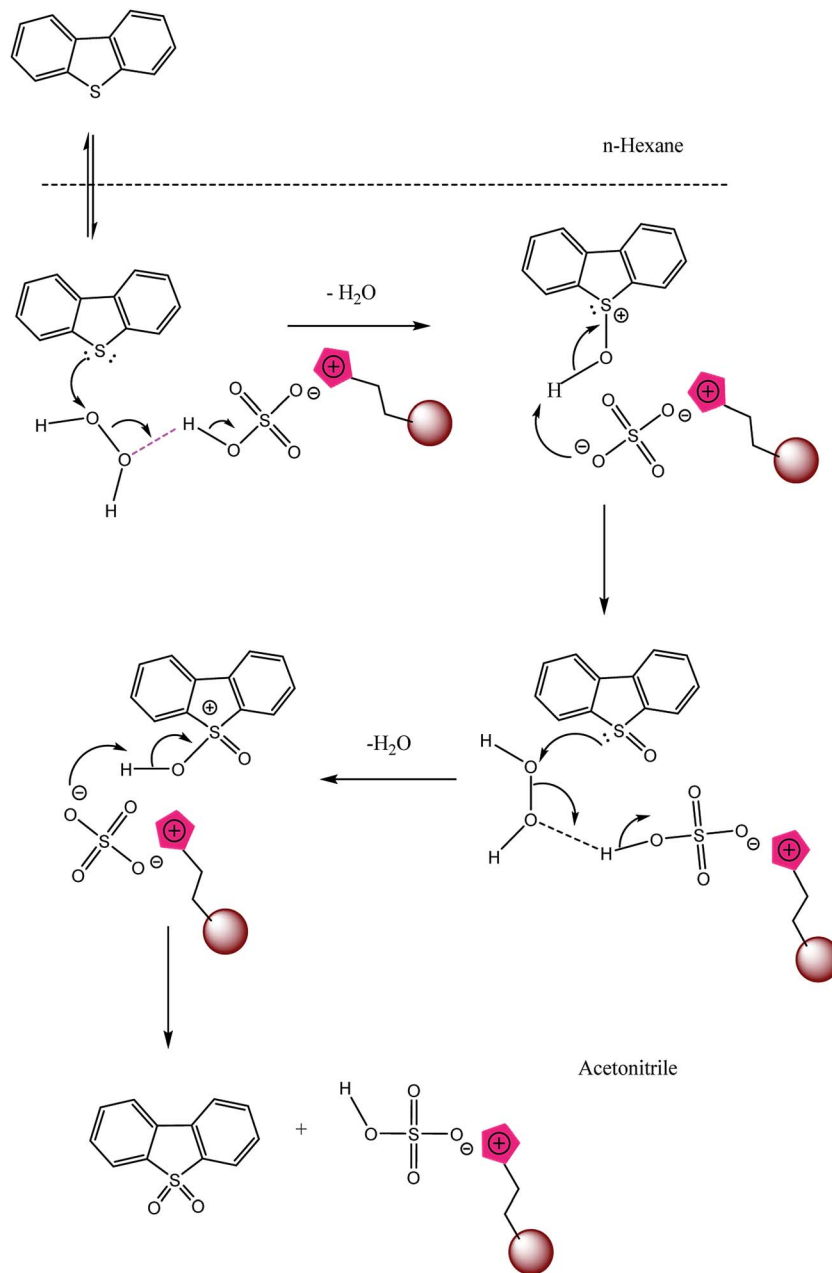
3.7 The suggested process and mechanism of DBT oxidation by $Fe_3O_4@SiO_2$–Mim–FeCl$_4$

The Fe^{3+} in $Fe_3O_4@SiO_2$–Mim–FeCl$_4$ and H_2O_2 formed a Fenton-like reagent because $[FeCl_4]^-$ can dissociate Fe^{3+}.[27,28,57,58] H_2O_2 can be decomposed into active hydroxyl radicals (HO•) that are strong oxidizing agents for DBT (eqn (1)–(3)).
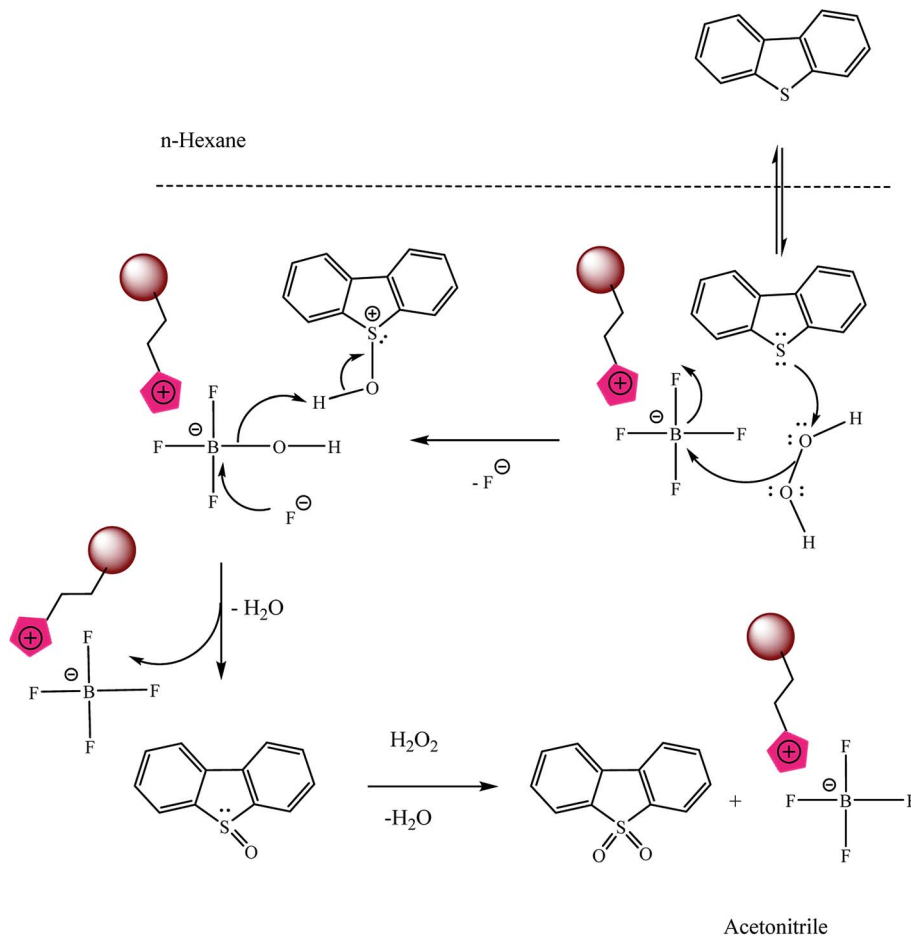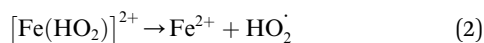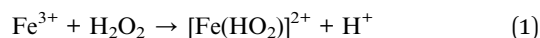

Scheme 4 The suggested mechanism of DBT oxidation by $Fe_3O_4@SiO_2$–Mim-BF$_4$.

Scheme 5 The suggested mechanism of DBT oxidation by $Fe_3O_4@SiO_2-Mim-HSO_4$.

$$Fe^{3+} + H_2O_2 \rightarrow [Fe(HO_2)]^{2+} + H^+ \tag{1}$$

$$[Fe(HO_2)]^{2+} \rightarrow Fe^{2+} + HO_2^{\cdot} \tag{2}$$

$$Fe^{2+} + H_2O_2 \rightarrow Fe^{3+} + HO^{\cdot} + OH^- \tag{3}$$

Another possible mechanism was illustrated in the Scheme 6:

In the following sections influence of some effective factors on desulfurization of model oil including the amount of catalyst, the amount of H_2O_2, and time were examined. The results were discussed.
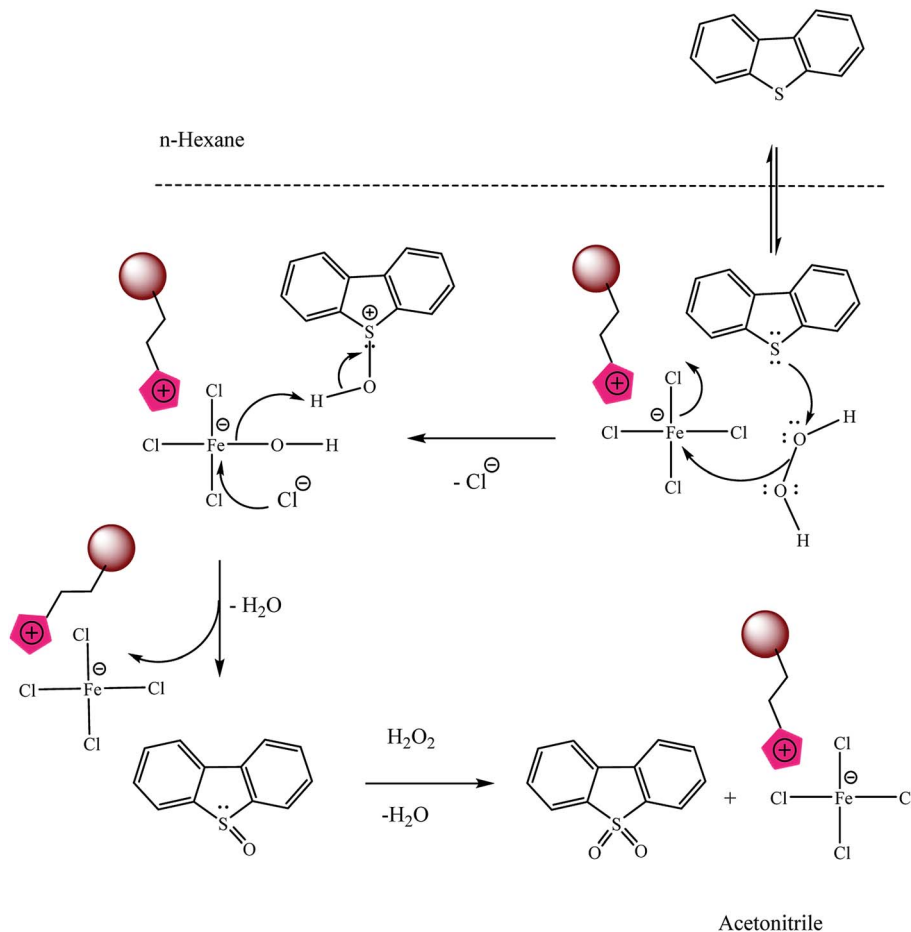
3.8 The amount of H_2O_2 effect on DBT oxidative removal

The oxidation of DBT under various H_2O_2 volume was conducted at 40 °C to study the effect of the dosage of oxidant on the oxidative properties. As shown in Fig. 8 by increasing the amount of H_2O_2, DBT oxidation growth.

3.9 Effect of the amount of the catalyst on DBT removal

The catalysts amount effect on desulfurization is shown in Fig. 9. The results indicated that the amount of the catalyst had a vital effect on the oxidation of DBT. For tree type of catalyst by increasing the amount of catalyst from 0.05 g to 0.1 g the

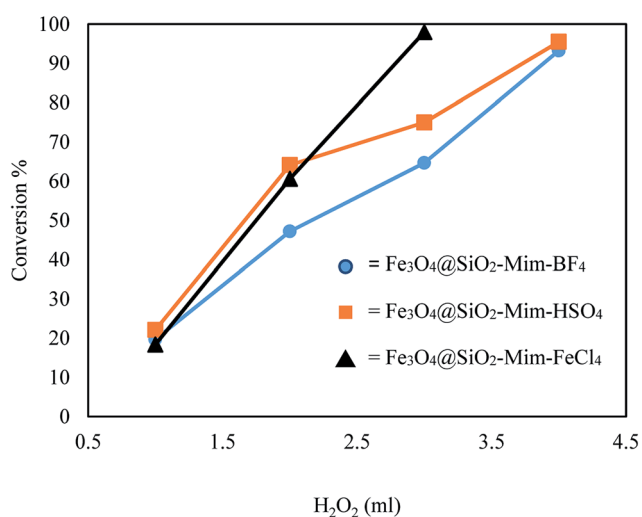**Scheme 6** The suggested mechanism of DBT oxidation by $Fe_3O_4@SiO_2-Mim-FeCl_4$.

Fig. 8 The effect of the amount of H_2O_2 on the conversation of DBT. Experimental conditions: amount of catalyst: 0.1 g, time: 60 minutes, temperature: 313 K.
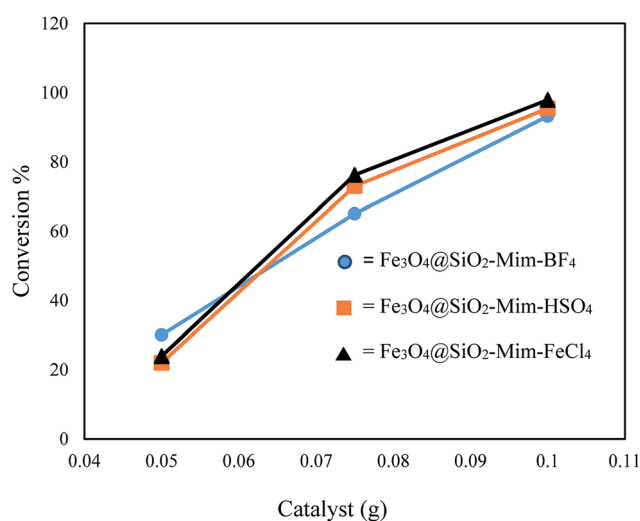

Fig. 9 The effect of the amount of catalyst on the conversation of DBT. Experimental conditions: amount of H_2O_2: 4 mL, time: 60 minutes, temperature: 313 K.

percent of DBT oxidation increase. Obviously, the excessive catalyst was not necessary and economical in the process. Thus, 0.1 g was chosen as the most suitable quantity in this study.

3.10 Effect of reaction time on oxidative removal of DBT

The DBT oxidation *versus* reaction time was determined according to the following equation (eqn (4)), where C_0 is the

concentration at time zero and C_t is the DBT concentration at the time.

$$C_{DBT} = \frac{C_0 - C_t}{C_t} \qquad (4)$$

As indicated in the graph conversion of DBT increased over time (Fig. 10).

The oxidative desulfurization efficiency were increased with increasing temperature. Sulfur removal reached to near 100% at 328 K in 60 min. Removal of DBT can be reached at 298 and 313 K in 60 min to 70.20 and 98% respectively. Therefore, 40 °C was chosen in the present study because of the concentration of hydrogen peroxide decreases due to nonproductive decomposition at high temperature (Fig. 11).[13]
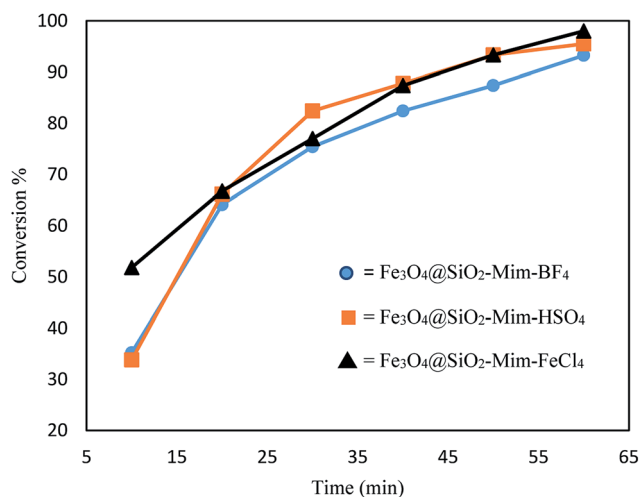

Fig. 10 The effect of the time on the conversation of DBT. Experimental conditions: amount of catalyst: 0.1 g, amount of H$_2$O$_2$: 4 mL, temperature: 313 K.
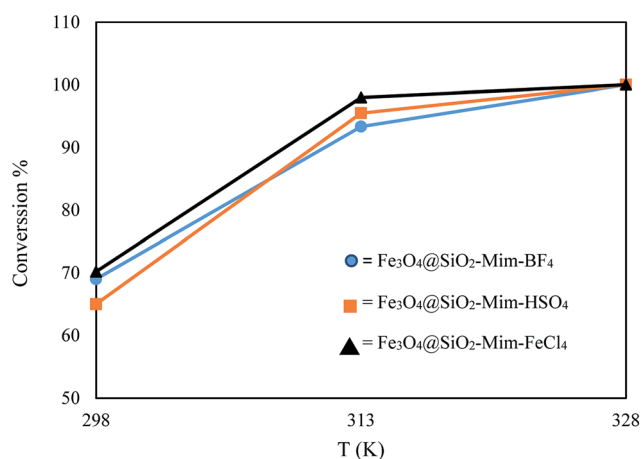

Fig. 11 The effect of temperature on the conversation of DBT. Experimental conditions: amount of catalyst: 0.1 g, amount of H$_2$O$_2$: 4 mL, time: 60 minutes.
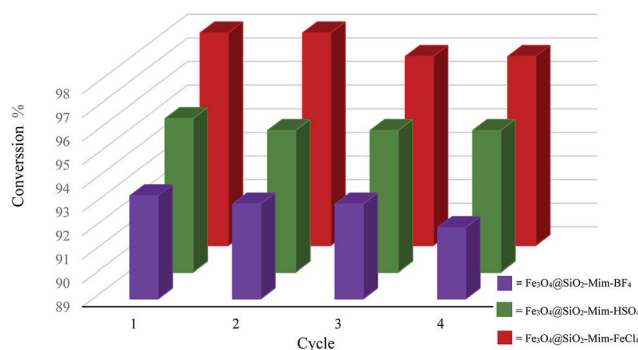

Fig. 12 Recycling of catalysts. Experimental conditions: amount of catalyst: 0.1 g, amount of H$_2$O$_2$: 4 mL, time: 60 minutes, temperature: 313 K.

3.11 Recycling of the catalysts

To further investigation the stability of catalysts, a series of catalyst recycle and reuse experiments for the DBT oxidation were conducted. Then a new reaction setup was accomplished with the fresh solvent and reactants under the same conditions. These catalysts can be easily recycled for further use because of its magnetism. Over four times of the recycle experiments conversion percentage has not changed much (Fig. 12). The high stability and excellent reusability of the catalyst can be contributed to the strong electrostatic interaction between the imidazolium ring and anionic moiety.

4. Conclusion

The main focus of the present research was concerned with achieving the efficient and feasible protocol for oxidative removal of DBT. Accordingly, we synthesized a series of Fe$_3$O$_4$-supported imidazolium-based Lewis or Brønsted acidic ionic liquids and applied as polar and nanomagnetic heterogeneous catalyst for oxidative desulfurization of dibenzothiophene from n-hexane as model oil phase in n-hexane/acetonitrile biphasic system. The order of catalysts performance was Fe$_3$O$_4$@SiO$_2$–Mim–FeCl$_4$ > Fe$_3$O$_4$@SiO$_2$–Mim-HSO$_4$ > Fe$_3$O$_4$@SiO$_2$–Mim-BF$_4$, the reason for this was that interaction between [FeCl$_4$]$^-$ moiety and oxygen of H$_2$O$_2$ was stronger than the others. Finally, regeneration and subsequent recycling of Lewis or Brønsted acidic methylimidazolium ionic liquid-functionalized Fe$_3$O$_4$@-SiO$_2$ nanoparticles have been investigated. The results showed that these catalysts could be used as promising catalysts for the oxidative desulfurization of future industrial application due to their higher desulfurization rates and easy separation by an external magnetic field.

Acknowledgements

References

1 X. Ma, K. Sakanishi and I. Mochida, *Ind. Eng. Chem. Res.*, 1994, **33**, 218–222.

2 A. Srivastav and V. C. Srivastava, *J. Hazard. Mater.*, 2009, **170**, 1133–1140.

3 X. Ma, L. Sun and C. Song, *Catal. Today*, 2002, **77**, 107–116.

4 S. Zhang, Q. Zhang and Z. C. Zhang, *Ind. Eng. Chem. Res.*, 2004, **43**, 614–622.

5 X. Wang, H. Wan, M. Han, L. Gao and G. Guan, *Ind. Eng. Chem. Res.*, 2012, **51**, 3418–3424.

6 D. J. Monticello, *Curr. Opin. Biotechnol.*, 2000, **11**, 540–546.

7 B. H. Kim, H. Y. Kim, T. S. Kim and D. H. Park, *Fuel Process. Technol.*, 1995, **43**, 87–94.

8 X.-M. Yan, P. Mei, L. Xiong, L. Gao, Q. Yang and L. Gong, *Catal. Sci. Technol.*, 2013, **3**, 1985–1992.

9 J. Gao, W. Ma, L. Yuan, Y. Dai and C. Li, *Appl. Catal., A*, 2013, **467**, 187–195.

10 J. Zhang, A. Wang, Y. Wang, H. Wang and J. Gui, *Chem. Eng. J.*, 2014, **245**, 65–70.

11 X. Cui, D. Yao, H. Li, J. Yang and D. Hu, *J. Hazard. Mater.*, 2012, **205**, 17–23.

12 W. Jiang, W. Zhu, Y. Chang, Y. Chao, S. Yin, H. Liu, F. Zhu and H. Li, *Chem. Eng. J.*, 2014, **250**, 48–54.

13 H. Lü, W. Ren, H. Wang, Y. Wang, W. Chen and Z. Suo, *Appl. Catal., A*, 2013, **453**, 376–382.

14 W. Zhu, W. Huang, H. Li, M. Zhang, W. Jiang, G. Chen and C. Han, *Fuel Process. Technol.*, 2011, **92**, 1842–1848.

15 K. Yazu, Y. Yamamoto, T. Furuya, K. Miki and K. Ukegawa, *Energy Fuels*, 2001, **15**, 1535–1536.

16 A. A. Gulam Gaush Zeelani, A. Dhakad, G. Gupta and S. L. Pal, *Int. J. Eng. Res. Tech.*, 2016, **3**, 331–336.

17 L. Tang, G. Luo, M. Zhu, L. Kang and B. Dai, *J. Ind. Eng. Chem.*, 2013, **19**, 620–626.

18 W.-H. Lo, H.-Y. Yang and G.-T. Wei, *Green Chem.*, 2003, **5**, 639–642.

19 L. Chen, S. Guo and D. Zhao, *Chin. J. Chem. Eng.*, 2007, **15**, 520–523.

20 G.-N. Yun and Y.-K. Lee, *Fuel Process. Technol.*, 2013, **114**, 1–5.

21 C. Shen, Y. J. Wang, J. H. Xu and G. S. Luo, *Chem. Eng. J.*, 2015, **259**, 552–561.

22 F. A. Duarte, P. d. A. Mello, C. A. Bizzi, M. A. G. Nunes, E. M. Moreira, M. S. Alencar, H. N. Motta, V. L. Dressler and É. M. M. Flores, *Fuel*, 2011, **90**, 2158–2164.

23 T. Welton, *Chem. Rev.*, 1999, **99**, 2071–2084.

24 M. Armand, F. Endres, D. R. MacFarlane, H. Ohno and B. Scrosati, *Nat. Mater.*, 2009, **8**, 621–629.

25 R. Abro, A. A. Abdeltawab, S. S. Al-Deyab, G. Yu, A. B. Qazi, S. Gao and X. Chen, *RSC Adv.*, 2014, **4**, 35302–35317.

26 A. W. Bhutto, R. Abro, S. Gao, T. Abbas, X. Chen and G. Yu, *J. Taiwan Inst. Chem. Eng.*, 2016, **62**, 84–97.

27 F.-t. Li, B. Wu, R.-h. Liu, X.-j. Wang, L.-j. Chen and D.-s. Zhao, *Chem. Eng. J.*, 2015, **274**, 192–199.

28 Y. Nie, Y. Dong, L. Bai, H. Dong and X. Zhang, *Fuel*, 2013, **103**, 997–1002.

29 X. Chen, D. Song, C. Asumana and G. Yu, *J. Mol. Catal. A: Chem.*, 2012, **359**, 8–13.

30 J. Wang, D. Zhao and K. Li, *Energy Fuels*, 2009, **23**, 3831–3834.

31 W. Zhang, K. Xu, Q. Zhang, D. Liu, S. Wu, F. Verpoort and X.-M. Song, *Ind. Eng. Chem. Res.*, 2010, **49**, 11760–11763.

32 H. Gao, C. Guo, J. Xing, J. Zhao and H. Liu, *Green Chem.*, 2010, **12**, 1220–1224.

33 J. Zhang, A. Wang, X. Li and X. Ma, *J. Catal.*, 2011, **279**, 269–275.

34 J. Xiong, W. Zhu, H. Li, Y. Xu, W. Jiang, S. Xun, H. Liu and Z. Zhao, *AIChE J.*, 2013, **59**, 4696–4704.

35 W. Ding, W. Zhu, J. Xiong, L. Yang, A. Wei, M. Zhang and H. Li, *Chem. Eng. J.*, 2015, **266**, 213–221.

36 N. A. Khan, Z. Hasan and S. H. Jhung, *Chem.–Eur. J.*, 2014, **20**, 376–380.

37 W. Zhu, B. Dai, P. Wu, Y. Chao, J. Xiong, S. Xun, H. Li and H. Li, *ACS Sustainable Chem. Eng.*, 2015, **3**, 186–194.

38 Z. Wu, Z. Li, J. Wu, L. Wang, S. Lu, L. Wang, H. Wan and G. Guan, *Ind. Eng. Chem. Res.*, 2014, **53**, 3040–3046.

39 M. Esmaeilpour, J. Javidi and M. Zandi, *Mater. Res. Bull.*, 2014, **55**, 78–87.

40 P.-H. Li, B.-L. Li, H.-C. Hu, X.-N. Zhao and Z.-H. Zhang, *Catal. Commun.*, 2014, **46**, 118–122.

41 Z. Zhang, F. Zhang, Q. Zhu, W. Zhao, B. Ma and Y. Ding, *J. Colloid Interface Sci.*, 2011, **360**, 189–194.

42 Y. Chen, F. Zhang, Y. Fang, X. Zhu, W. Zhen, R. Wang and J. Ma, *Catal. Commun.*, 2013, **38**, 54–58.

43 M. Davudabadi Farahani and F. Shemirani, *Microchim. Acta*, 2012, **179**, 219–226.

44 X. Liu, X. Lu, Y. Huang, C. Liu and S. Zhao, *Talanta*, 2014, **119**, 341–347.

45 E. Santos, J. Albo and A. Irabien, *RSC Adv.*, 2014, **4**, 40008–40018.

46 W. Zhu, P. Wu, L. Yang, Y. Chang, Y. Chao, H. Li, Y. Jiang, W. Jiang and S. Xun, *Chem. Eng. J.*, 2013, **229**, 250–256.

47 D. Yang, J. Hu and S. Fu, *J. Phys. Chem. C*, 2009, **113**, 7646–7651.

48 W. Stöber, A. Fink and E. Bohn, *J. Colloid Interface Sci.*, 1968, **26**, 62–69.

49 T. Zeng, L. Yang, R. Hudson, G. Song, A. R. Moores and C.-J. Li, *Org. Lett.*, 2011, **13**, 442–445.

50 T. Yang, C. Shen, Z. Li, H. Zhang, C. Xiao, S. Chen, Z. Xu, D. Shi, J. Li and H. Gao, *J. Phys. Chem. B*, 2005, **109**, 23233–23236.

51 Z. Lei, Y. Li and X. Wei, *J. Solid State Chem.*, 2008, **181**, 480–486.

52 A. S. Amarasekara and O. S. Owereh, *Catal. Commun.*, 2010, **11**, 1072–1075.

53 M. Yamaura, R. L. Camilo, L. C. Sampaio, M. A. Macêdo, M. Nakamura and H. E. Toma, *J. Magn. Magn. Mater.*, 2004, **279**, 210–217.

54 X. Creary and E. D. Willis, *Org. Synth.*, 2005, **82**, 166–169.

55 K. Bahrami, M. M. Khodaei and P. Fattahpour, *Catal. Sci. Technol.*, 2011, **1**, 389–393.

56 M. M. Khodaei, K. Bahrami and M. Sheikh Arabi, *J. Sulfur Chem.*, 2010, **31**, 83–88.

57 J. Zhang, W. Zhu, H. Li, W. Jiang, Y. Jiang, W. Huang and Y. Yan, *Green Chem.*, 2009, **11**, 1801–1807.

58 J. Xiong, W. Zhu, H. Li, Y. Xu, W. Jiang, S. Xun, H. Liu and Z. Zhao, *AIChE J.*, 2013, **59**, 4696–4704.